Supporting Information

Highly Ordered Pd/CeO_x Inverse Opals for Alkaline Hydrogen Oxidation

*Michael Wilms[1,2], Arma Musa Yau[1,2], Ruby Susan Raju[1], Deya Sallaberry[1] and Mathilde Luneau[1,2]**

[1]Department of Chemistry and Chemical Engineering, Chalmers University of Technology, Gothenburg 412 96, Sweden

[2]Competence Centre for Catalysis (KCK), Chalmers University of Technology, Gothenburg 412 96, Sweden

*e-mail: mathilde.luneau@chalmers.se

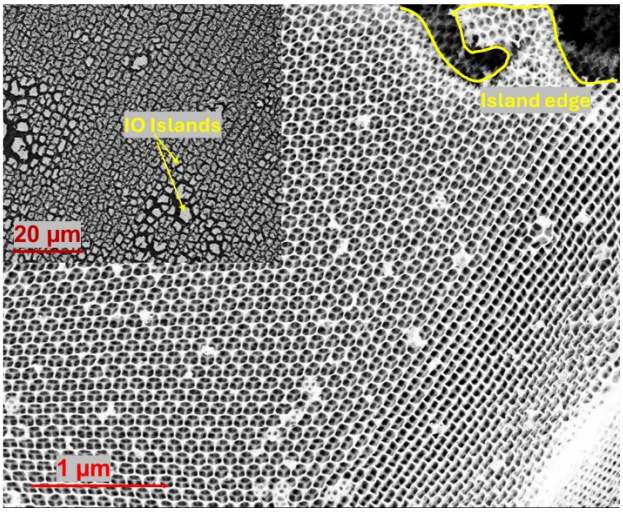

***Figure S 1**. SEM micrograph of inverse opal made using 510 nm polystyrene microspheres with high magnification (inset) image showing the "island formation" of the highly ordered IOs.*

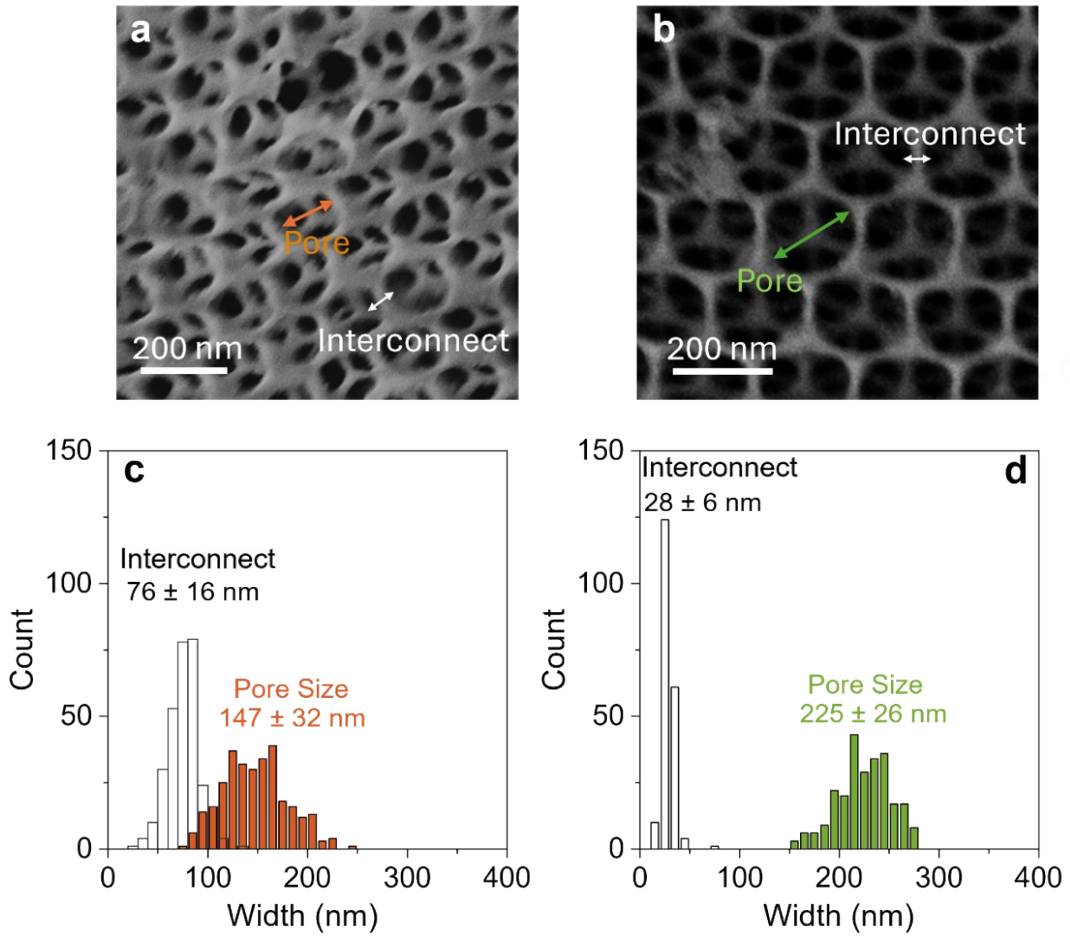

***Figure S 2**. (a, c) SEM micrograph of inverse opal made using 380 nm polystyrene microspheres indicating pore and backbone occurrences. (b, d) Histogram showing the measured pore size and backbone widths for 510 nm inverse opals. It was not possible to measure pore and backbone width distributions of the 104 nm IO due the pores being too small to accurately measure in SEM*

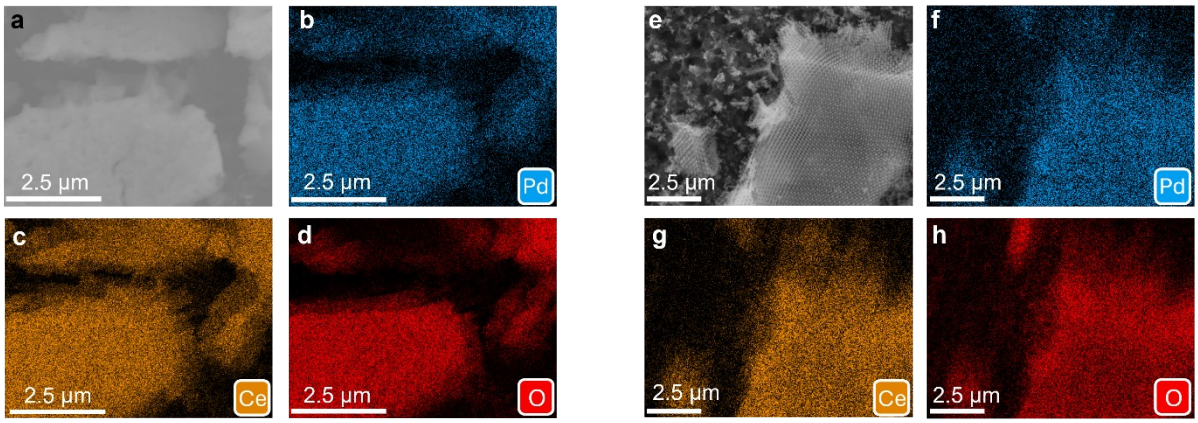

***Figure S 3**. SEM/EDX maps of (a-d) 104 nm (d-g) and 510 nm Pd/CeO_x IO showing uniform distribution of Pd throughout the porous CeO_x framework.*

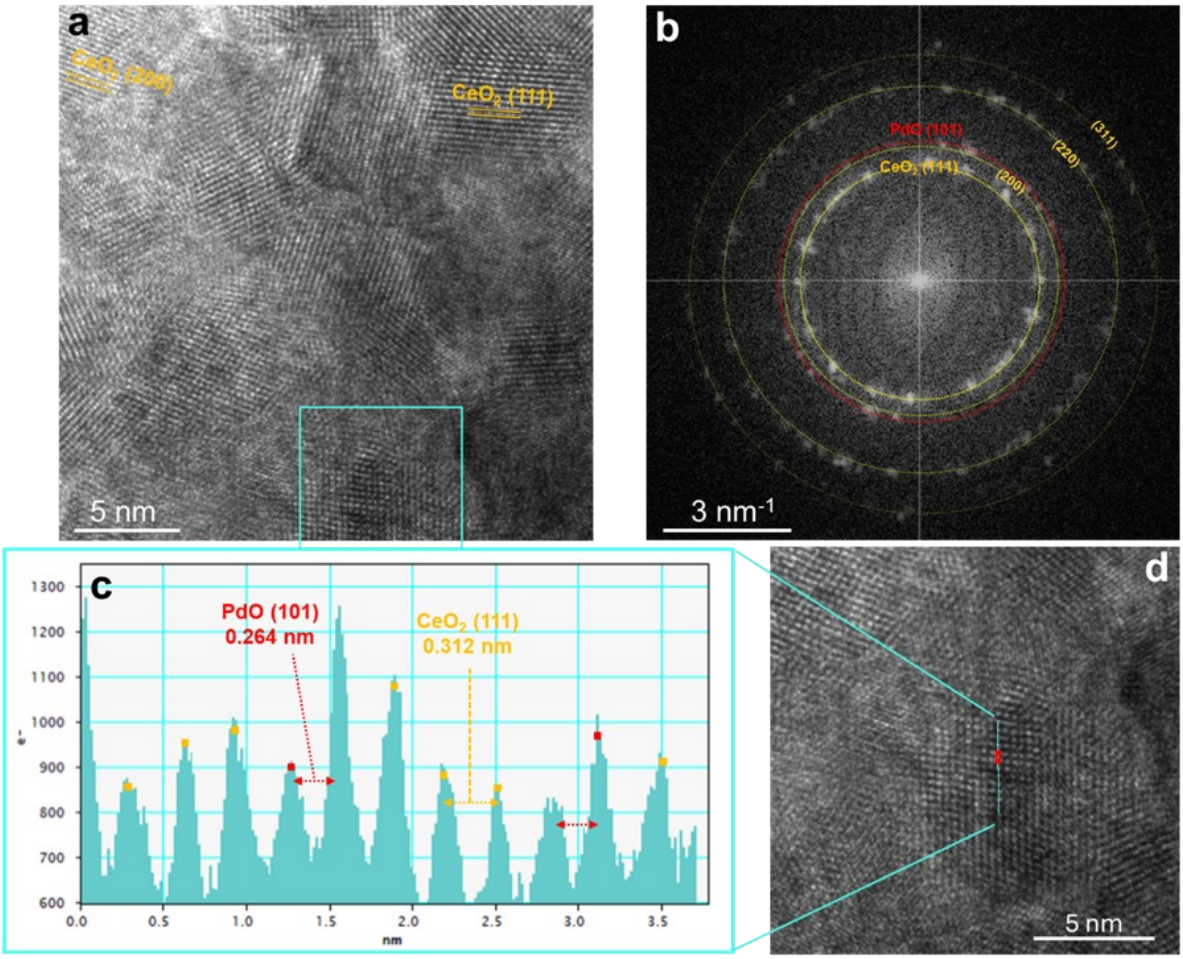

Figure S 4. *(a) HR-TEM of Pd/CeO_x 510 nm IO showing main lattice fringes of CeO_x (111) and (200). (b) FFT analysis of lattice fringes in HR-TEM showing diffraction rings of CeO_2 and PdO. (c, d) HR-TEM lattice fringe analysis of CeO_2 crystallite (blue square) showing Pd substitution within CeO_2 (111) lattice plane.*

Table S 1. *Elemental weight percentages of various Pd/CeO_x morphologies as determined by Energy-Dispersive X-ray Spectroscopy (EDX).*

Wt%	No Opal	104 nm	380 nm	510 nm
Ce	68.7	27.0	47.3	21.9
O	17.8	18.4	19.5	16.1
Pd	9.62	2.89	6.13	2.49
Pd/Ce	**0.140**	**0.107**	**0.130**	**0.114**

Table S 2. *Surface composition, Pd3d peak positions and FWHM of Pd/CeO_x IOs from XPS measurement and analysis.*

Morphology	Pd Species	Percentage (%)	$3d_{5/2}$ Position (eV)	$3d_{3/2}$ Position (eV)	FWHM (eV)
No Opal	Pd(0)	-	-	-	-
	PdO	81.89	336.30	341.60	1.60
	Pd-O-Ce	18.11	337.69	342.99	2.23
104 nm	Pd(0)	-	-	-	-
	PdO	51.85	335.93	341.23	1.60
	Pd-O-Ce	48.15	337.11	342.41	1.92
380 nm	Pd(0)	8.63	335.39	341.25	1.30
	PdO	64.39	335.99	341.27	1.60
	Pd-O-Ce	26.98	337.01	342.04	3.00
510 nm	Pd(0)	6.78	334.14	339.44	1.30
	PdO	55.20	335.94	341.24	1.60
	Pd-O-Ce	38.02	337.01	342.31	2.42

Effect of Calcination Conditions on Pd/CeO_x IOs

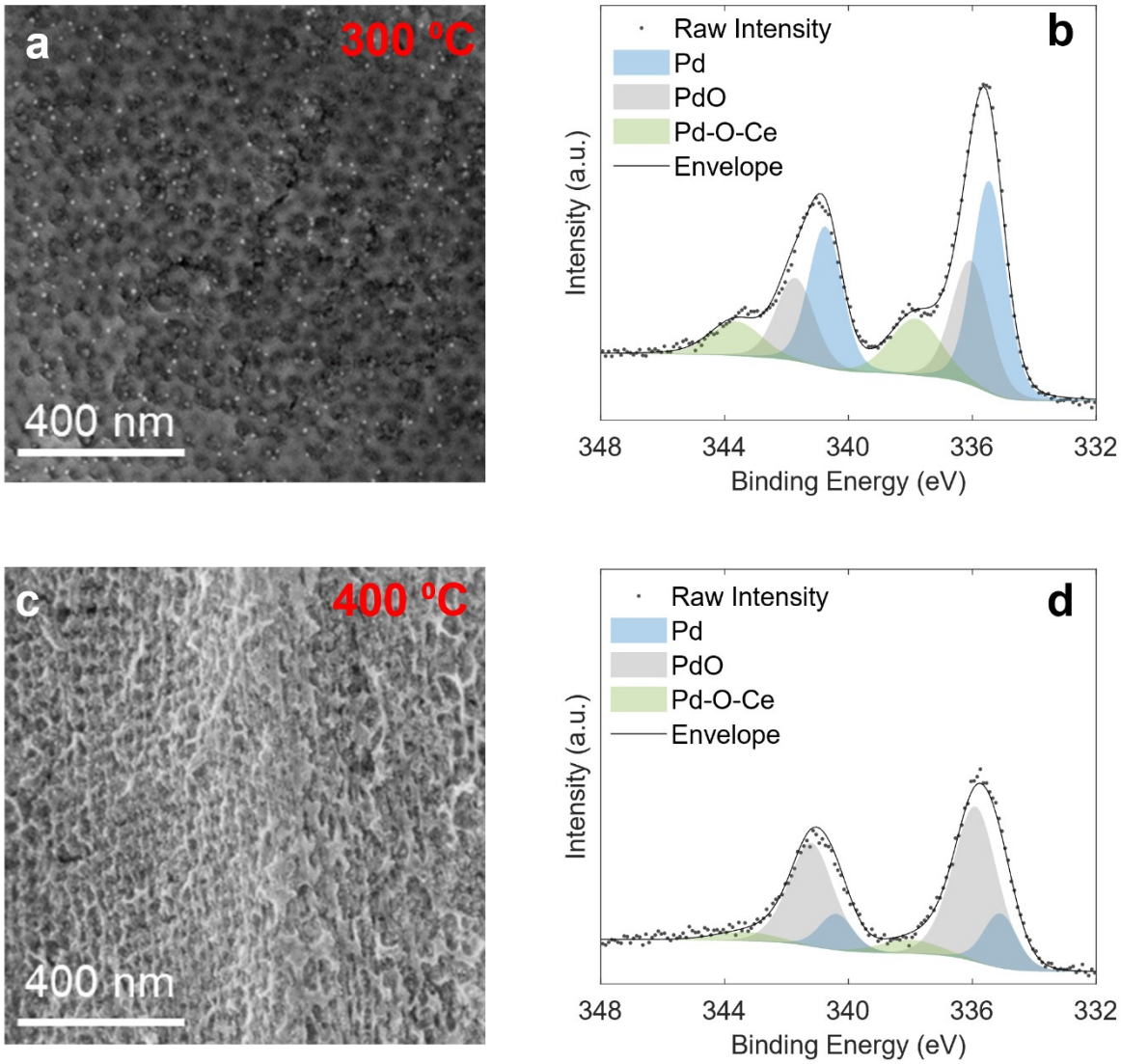

Figure S 5. (a, c) SEM micrograph of inverse opal made using 104 nm polystyrene microspheres calcined at different calcination temperatures using a ramp of 1 ºC/min ramp and (b, d) corresponding XPS Pd3d spectra.

The calcination conditions of Pd/CeO_x were found to heavily govern Pd dispersion and speciation in XPS. Calcination at 300 °C (1 ºC/min ramp) resulted in the formation of visible Pd nanoparticles with average diameters of approximately 20 nm, which was corroborated by the presence of a metallic Pd component in the XPS Pd 3d spectrum (**Figure S5a**, **c**). Note, the slow heating ramp employed for these samples led to poor-quality inverse opal structures. While ramp speed likely had less influence on Pd dispersion, it clearly affected the resulting IO morphology. Increasing the calcination temperature to 400 °C led to the disappearance of the majority of the Pd nanoparticles, with XPS analysis indicating only a minor residual metallic phase. For the 500 °C calcination temperature utilized throughout this study, no Pd

nanoparticles were observed via SEM. In this case, metallic Pd was detected only in the 380 nm and 510 nm IO samples as a small minority species (<10%).

Samples annealed in Argon at 500 °C also formed Pd nanoparticles (~20 nm) with visible aggregation also observed (**Figure S 10**). This nanoparticle formation was corroborated by XPS analysis (**Figure S 13**), suggesting that an oxidative environment during calcination at >500 ºC is critical for maintaining high Pd dispersion within the ceria framework.

Electrochemical Measurements

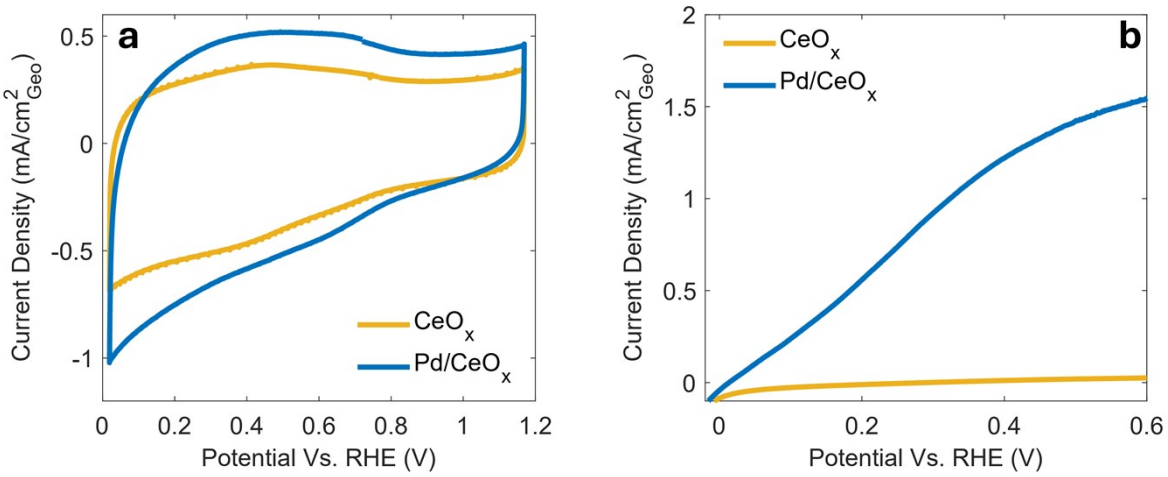

***Figure S 6**. (a) Cyclic voltammetry of CeO_x and Pd/CeO_x 104 nm inverse opal at a scan rate of 100 mV/s and in argon atmosphere in 0.1 M KOH electrolyte. (b) Anodic HOR sweeps at a scan rate of 5 mV/s at a rotation speed of 1600 RPM in saturated H_2 atmosphere in 0.1M KOH electrolyte.*

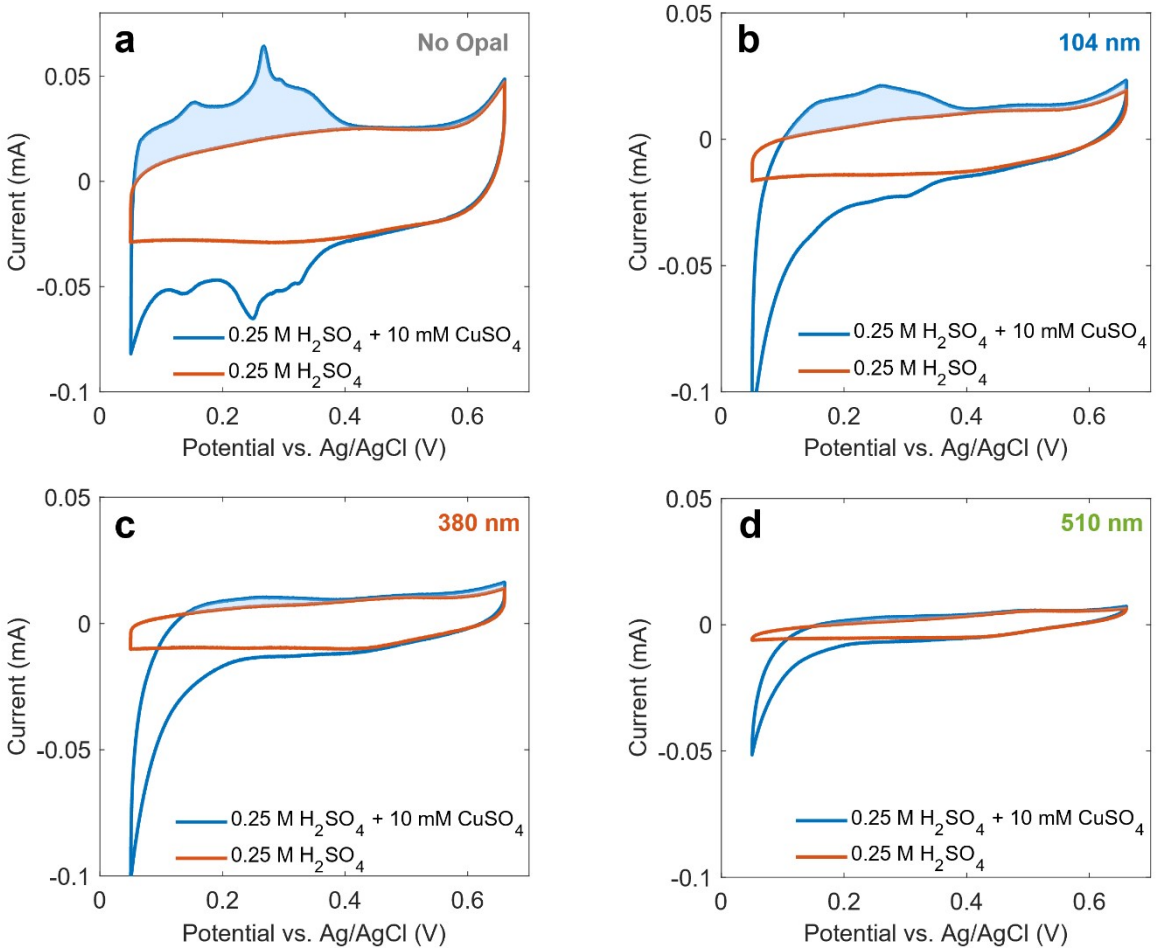

***Figure S 7 ~~3~~**. Cu UPD scanning curves of different Pd/CeO_x samples, recorded at a scan rate of 10 mV/s in argon atmosphere.*

***Table S 3**. Relative surface areas of IO electrodes estimated from capacitance in cyclic-voltammograms, assuming the geometric area of the non-templated (No opal) sample was 0.196 cm². The actual surface area of the no opal sample likely differed from the geometric area due to inherent surface roughness, therefore these values should be treated as relative estimates.*

Potential vs. RHE (V)	No opal	104 nm	380 nm	510 nm
-0.4	0.196	0.125	0.09	0.024
0.0	0.196	0.106	0.09	0.024

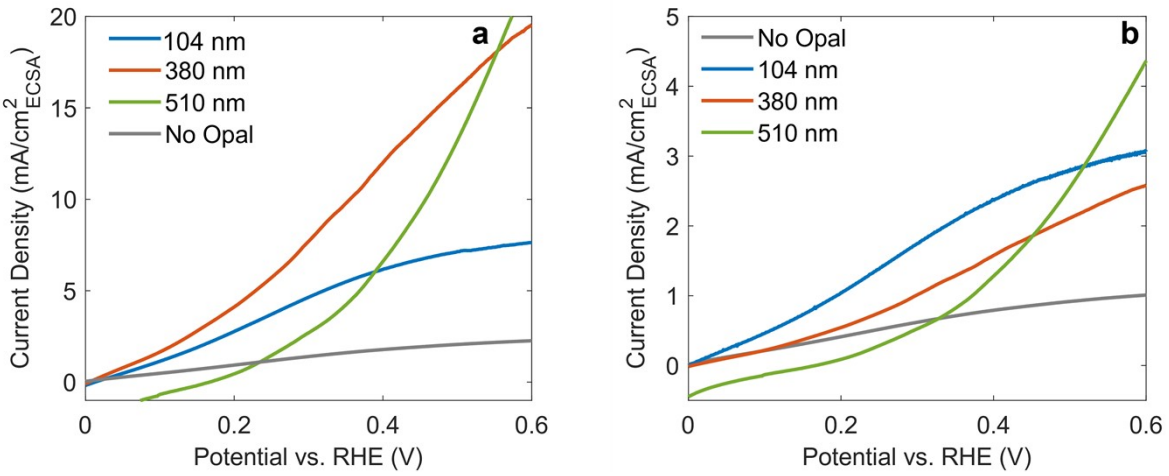

***Figure S 8**. ECSA Normalized HOR sweeps from (a) CuUPD and (b) cyclic voltammetry derived capacitance from samples shown in **Figure 4b**.*

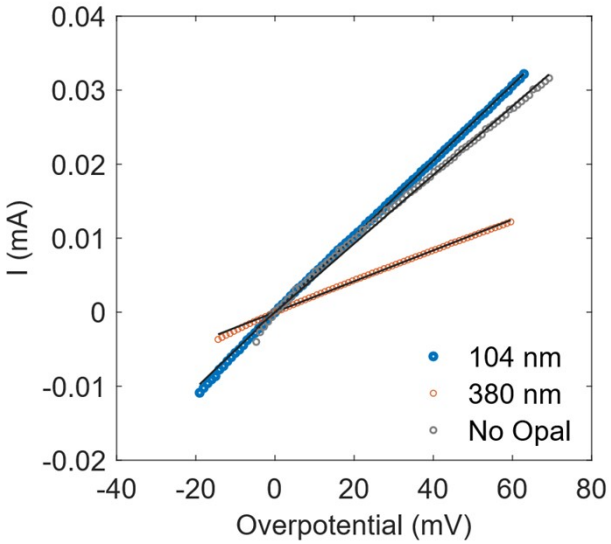

***Figure S 9**. HOR Micropolarization region of Pd/CeO_x IOs to estimate exchange current densities (j_o).*

Effect of Ar Annealing on Pd/CeO_x

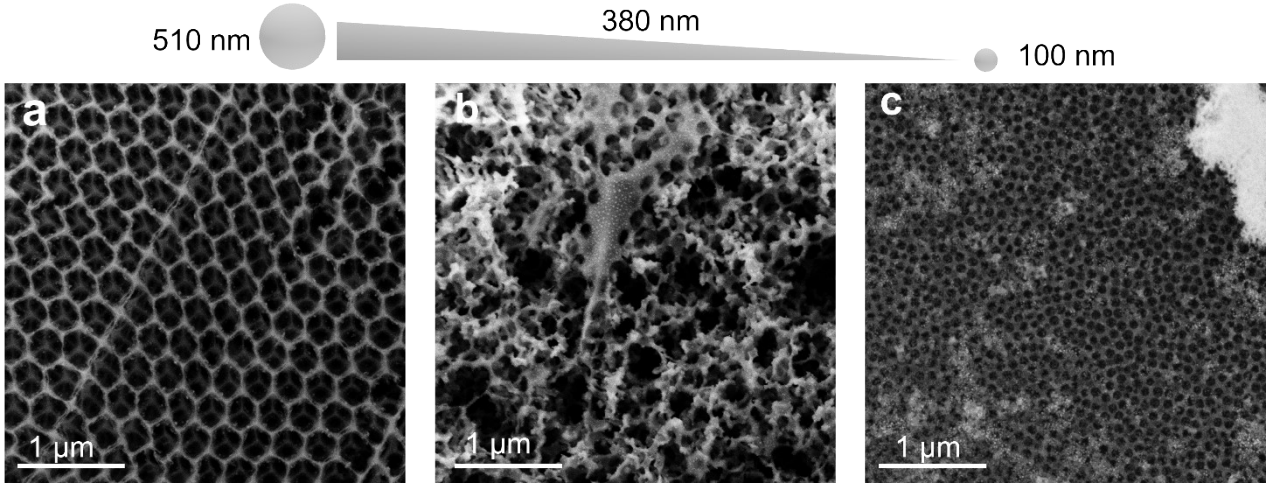

Figure S 10. *Highly ordered Pd/CeO_x inverse opals synthesized via template removal in argon as shown by SEM micrographs using polymer microsphere sizes of (a) 510 nm, (b) 330 nm and (c) 104 nm. The 380 nm IO is observed to have a more disordered pore network.*

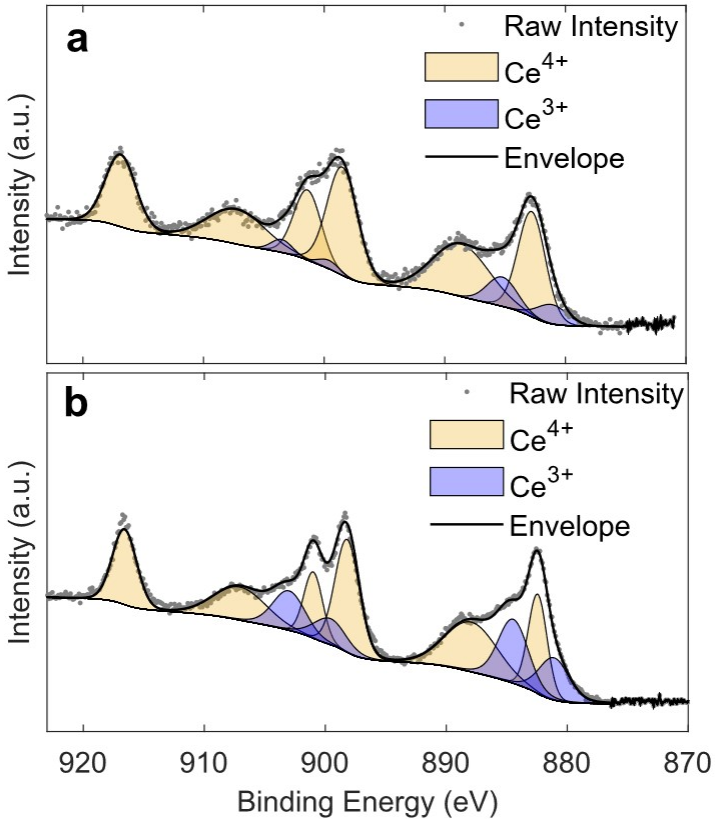

Figure S 11. *Cerium 3d XPS region of (**a**) air calcined 104 nm IO and (**b**) argon annealed 104 nm IO.*

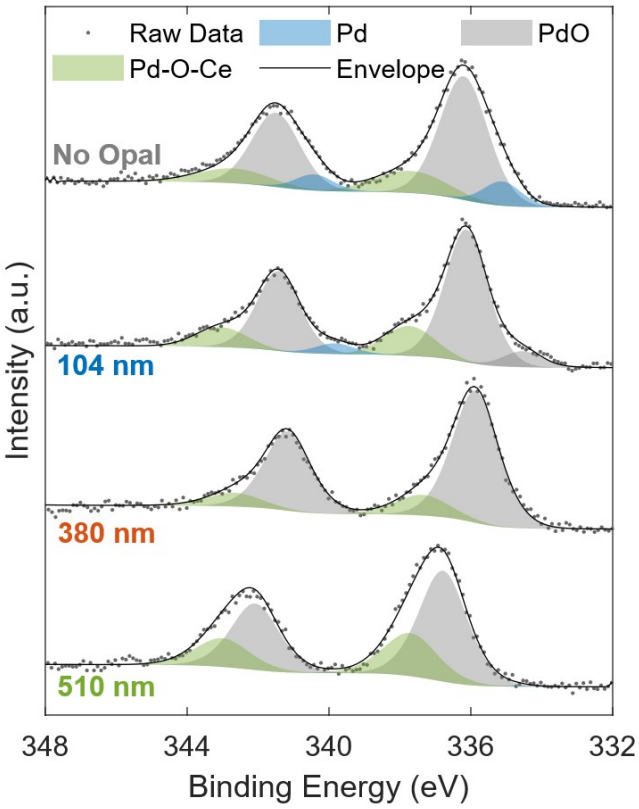

Figure S 12. *Pd3d XPS region of (a) No opal, (b) 104nm, (c) 380 nm and (d) 510 nm Pd/CeO_x calcined in air. A 10 wt% nominal Pd loading was utilized for all samples.*

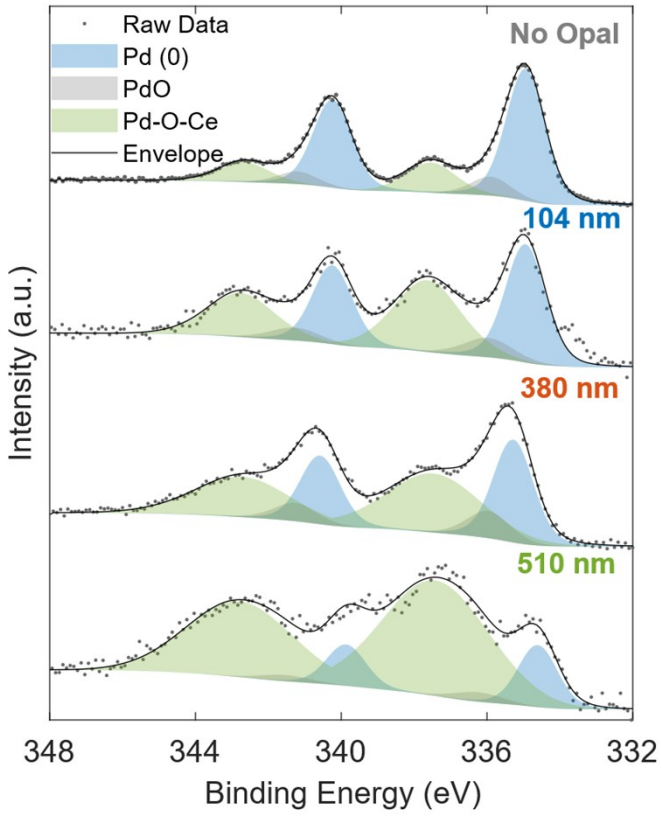

Figure S 13. *Pd3d XPS region of (a) No opal, (b) 104nm, (c) 380 nm and (d) 510 nm Pd/CeO_x annealed in argon atmosphere. A 10 wt% nominal Pd loading was utilized for all samples.*

Table S 4. *Surface composition, Pd3d peak positions and FWHM of air calcined Pd/CeO_x from XPS measurement and analysis. A 10 wt% nominal Pd loading was utilized for all samples.*

Morphology	Pd Species	Percentage (%)	$3d_{5/2}$ Position (eV)	$3d_{3/2}$ Position (eV)	FWHM (eV)
No Opal	Pd(0)	11.82	335.12	340.42	1.26
	PdO	69.23	336.20	341.50	1.60
	Pd-O-Ce	18.95	337.69	342.70	2.23
104 nm	Pd(0)	9.00	334.54	339.84	1.30
	PdO	71.62	336.13	341.43	1.42
	Pd-O-Ce	19.38	337.74	342.66	1.68
380 nm	Pd(0)	-	-	-	-
	PdO	83.91	335.89	341.19	1.53
	Pd-O-Ce	16.09	337.36	342.04	1.80
510 nm	Pd(0)	0.46	334.65	339.95	0.91
	PdO	68.35	336.78	342.08	1.60
	Pd-O-Ce	31.19	337.71	343.01	1.80

Table S 5*. Surface composition, Pd3d peak positions and FWHM of argon annealed Pd/CeO_x from XPS measurement and analysis. A 10 wt% nominal Pd loading was utilized for all samples.*

Morphology	Pd Species	Percentage (%)	$3d_{5/2}$ Position (eV)	$3d_{3/2}$ Position (eV)	FWHM (eV)
No Opal	Pd(0)	70.50	334.94	340.24	1.26
	PdO	9.96	335.90	341.20	1.30
	Pd-O-Ce	19.54	337.53	342.68	1.62
104 nm	Pd(0)	41.24	334.94	340.18	1.20
	PdO	9.32	335.97	341.27	1.60
	Pd-O-Ce	49.45	337.63	342.76	2.17
380 nm	Pd(0)	44.48	335.39	340.69	1.30
	PdO	4.64	335.97	341.27	1.60
	Pd-O-Ce	50.87	337.31	342.61	3.18
510 nm	Pd(0)	17.29	334.63	339.89	1.30
	PdO	3.09	336.23	341.53	1.55
	Pd-O-Ce	79.62	337.42	342.79	3.43

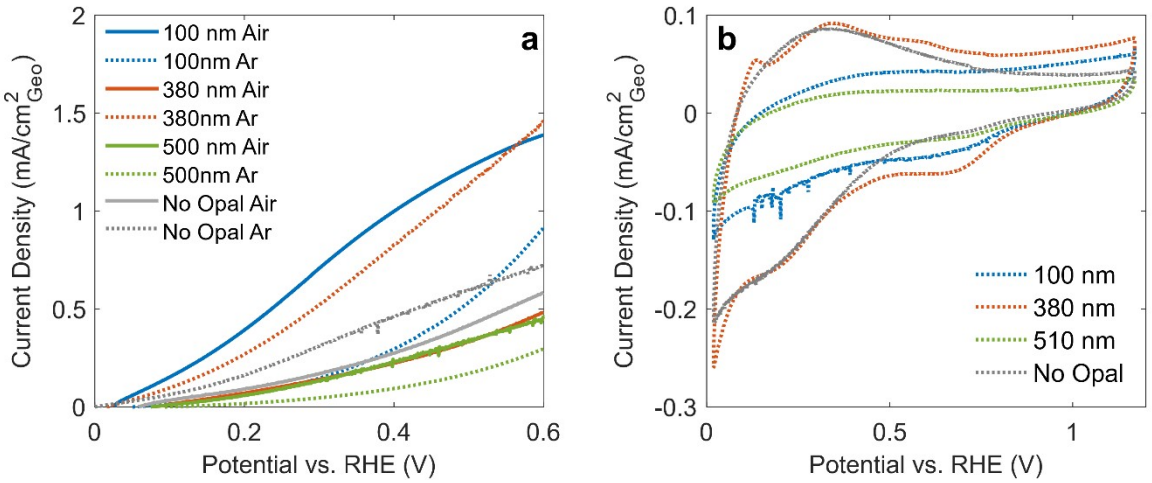

Figure S 14. *(**a**) Anodic HOR sweeps of air calcined anodes (lines) and Ar annealed anodes (broken lines) recorded using a scan rate of 5mV/s at a RDE rotation speed of 1600 RPM under saturated H_2 atmosphere. (**b**) Cyclic voltammogram of anodes annealed in argon recorded at 100 mV/s under argon atmosphere. A 10 wt% nominal Pd loading was utilized for all samples.*

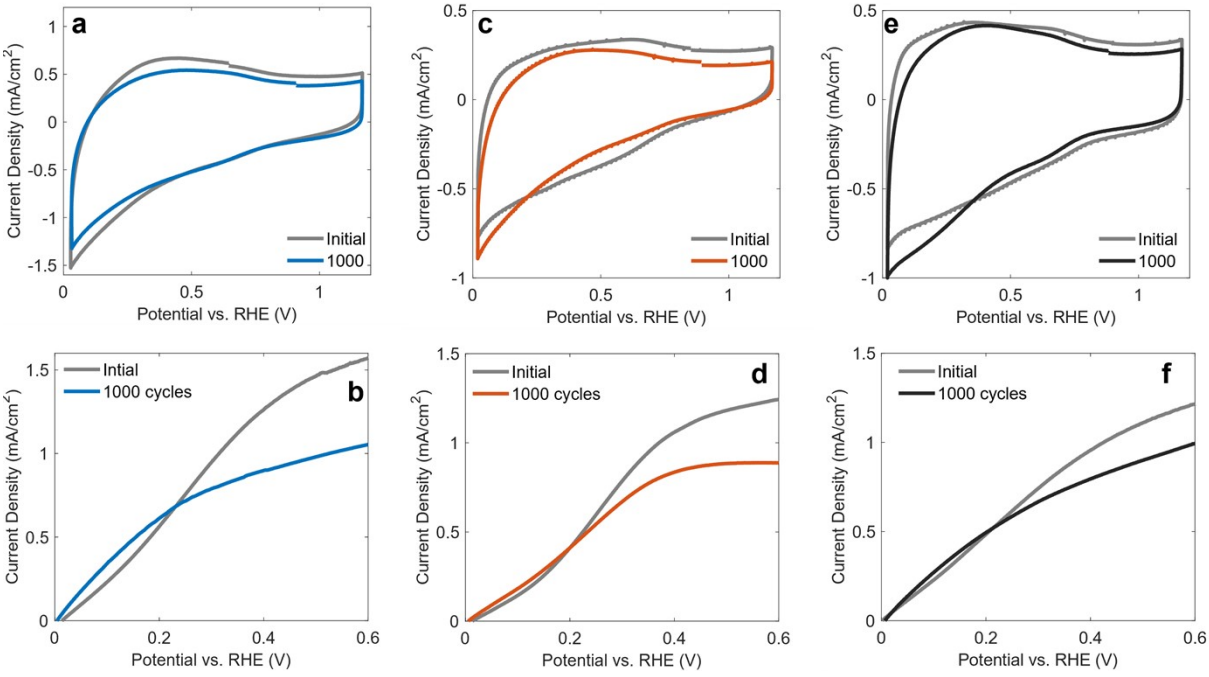

Figure S 15*. Cyclic voltammograms (initial and 1000th cycle) and anodic HOR sweeps before potential cycling (initial) and after 1000th potential cycle for 104 nm (**a**-**b**), 380 nm (**c**-**d**) and no opal (**e**-**f**) Pd/CeO_x.*

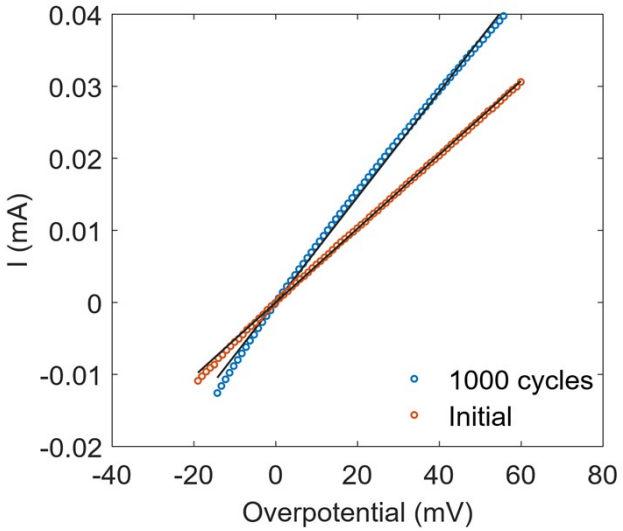

***Figure S 16**. HOR micropolarization region of 104 nm Pd/CeO_x IOs before and after potential cycling.*

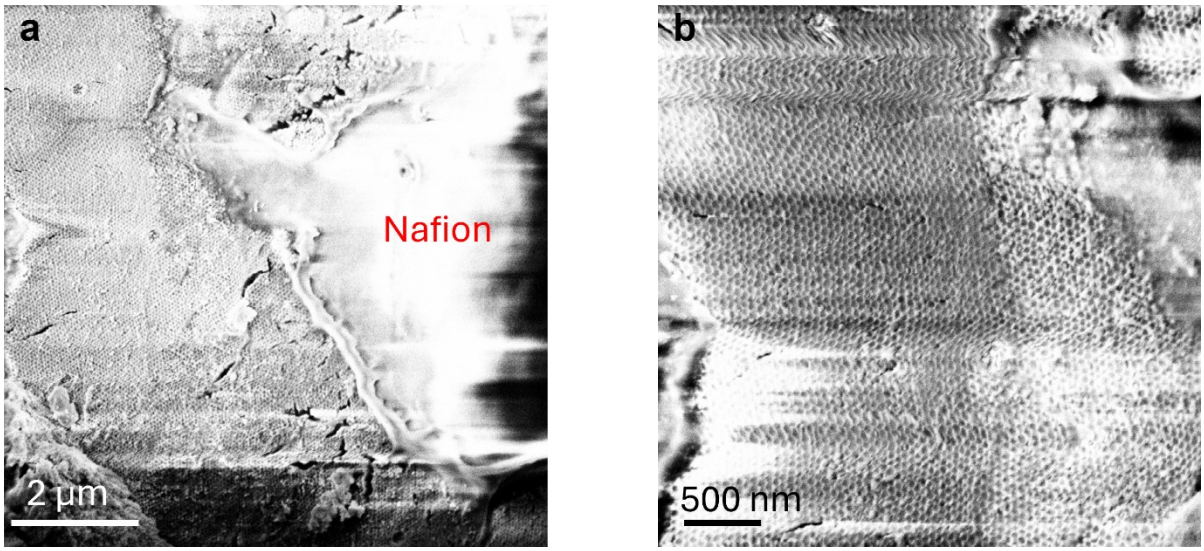

***Figure S 17**. SEM images of 104 nm Pd/CeO_x IO after 1000 CV cycles clearly showing the preservation of the mesoporous structure. The smooth area and strong charging effects are due to nafion deposition before electrochemical testing.*